BJP British Journal of Pharmacology

DOI:10.1111/bph.12681
www.brjpharmacol.org

RESEARCH PAPER

Reactive oxygen species induce MMP12-dependent degradation of collagen 5 and fibronectin to promote the motility of human umbilical cord-derived mesenchymal stem cells

Seung Pil Yun[1]*, Sei-Jung Lee[1]*, Sang Yub Oh[1], Young Hyun Jung[1], Jung Min Ryu[1], Han Na Suh[1], Mi Ok Kim[1], Keon Bong Oh[2] and Ho Jae Han[1]

[1]*Department of Veterinary Physiology, College of Veterinary Medicine, Research Institute for Veterinary Science* and *BK21 PLUS Program for Creative Veterinary Science Research, Seoul National University, Seoul, Korea, and* [2]*Animal Biotechnology Division, National Institute of Animal Science, RDA, Suwon, Korea*

Correspondence
Ho Jae Han, Department of Veterinary Physiology, College of Veterinary Medicine, Seoul National University, Gwanak-ro, Gwanak-gu, Seoul 151-742, South Korea. E-mail: hjhan@snu.ac.kr

*SPY and S-JL contributed equally to this paper.

Keywords
umbilical cord blood-derived mesenchymal stem cells; hydrogen peroxide; MMP; extracellular matrix proteins; motility; skin wound healing

Received
13 November 2013
Revised
26 February 2014
Accepted
5 March 2014

BACKGROUND AND PURPOSE

Reactive oxygen species (ROS) are potent regulators of stem cell behaviour; however, their physiological significance as regards MMP-mediated regulation of the motility of human umbilical cord blood-derived mesenchymal stem cells (UCB-MSCs) has not been characterized. In the present study, we investigated the role of hydrogen peroxide (H_2O_2) and associated signalling pathways in promoting UCB-MSCs motility.

EXPERIMENTAL APPROACH

The regulatory effects of H_2O_2 on the activation of PKC, MAPKs, NF-κB and β-catenin were determined. The expressions of MMP and extracellular matrix proteins were examined. Pharmacological inhibitors and gene-specific siRNA were used to identify the signalling pathways of H_2O_2 that affect UCB-MSCs motility. An experimental skin wound-healing model was used to confirm the functional role of UCB-MSCs treated with H_2O_2 in ICR mice.

KEY RESULTS

H_2O_2 increased the motility of UCB-MSCs by activating PKCα via a calcium influx mechanism. H_2O_2 activated ERK and p38 MAPK, which are responsible for the distinct activation of transcription factors NF-κB and β-catenin. UCB-MSCs expressed eight MMP genes, but only MMP12 expression was uniquely regulated by NF-κB and β-catenin activation. H_2O_2 increased the MMP12-dependent degradation of collagen 5 (COL-5) and fibronectin (FN) associated with UCB-MSCs motility. Finally, topical transplantation of UCB-MSCs treated with H_2O_2 enhanced skin wound healing in mice.

CONCLUSIONS AND IMPLICATIONS

H_2O_2 stimulated UCB-MSCs motility by increasing MMP12-dependent degradation of COL-5 and FN through the activation of NF-κB and glycogen synthase kinase-3β/β-catenin, which is critical for providing a suitable microenvironment for MSCs transplantation and re-epithelialization of skin wounds in mice.

Abbreviations

COL, collagen; ECM, extracellular matrix; FN, fibronectin; GSK-3β, glycogen synthase kinase 3β; ROS, reactive oxygen species; UCB-MSCs, umbilical cord blood-derived mesenchymal stem cells

Introduction

Reactive oxygen species (ROS), essential regulators of cell metabolism, are also known to be toxic radicals that can damage macromolecules (Cuzzocrea *et al.*, 2001; Lambeth *et al.*, 2008). However, results from a recent study suggested that cellular ROS are tightly regulated to prevent tissue damage and that they play a critical role as second messengers in several self-renewing tissues and thereby regulate cellular activities (Le Belle *et al.*, 2011; Morimoto *et al.*, 2013). Specifically, it is known that injected or transplanted stem cells are exposed to long-term hypoxic conditions in which ROS inevitably causes alterations in their behaviour. However, the functional role of ROS in stem cells is still largely unknown. Of all the ROS so far identified, hydrogen peroxide (H_2O_2) is the most stable oxidant and it can diffuse across cellular membranes through water channels (Henzler and Steudle, 2000). Many studies have established a physiological role for H_2O_2 in signal transduction pathways, ion channel activation and transcription factor regulation (Burdon, 1995; Sundaresan *et al.*, 1995; Irani *et al.*, 1997). Given that H_2O_2 plays a critical role in wound healing (Allaoui *et al.*, 2009; Pan *et al.*, 2011), it is important to clarify how H_2O_2 regulates stem cell motility in a wounded area before stem cells are used in regeneration strategies.

PKC and MAPK are important kinases responsible for the growth and survival of stem cells (Lee *et al.*, 2009). In embryonic stem cells (ESCs), H_2O_2 is able to activate conventional, novel or atypical PKCs and so promote the activation of MAPKs (Lee *et al.*, 2009). In addition, it has been shown that phosphorylation of PKC and MAPK is required for the regulation of stem cell functions through the facilitation of multifunctional transcription factors, such as NF-κB and β-catenin (Yang *et al.*, 2012; Lee do *et al.*, 2013; Priyanka *et al.*, 2013). However, the coordination of signal transduction cascades downstream of H_2O_2 via effector molecules is still unclear. To our knowledge, the mechanism of the migration-promoting effects of tissue-affinitive H_2O_2 in stem cells used for therapeutic applications has not been studied. However, there are a few reports indicating that ROS regulate adhesion/migration-related proteins such as MMP and extracellular matrix (ECM) in cells in wounded areas (Loo *et al.*, 2012; Eble and Figueiredo de Rezende, 2014). MMPs are the main enzymes responsible for the degradation of ECM components (see Alexander *et al.*, 2013), and more than 26 MMPs have been identified (Peng *et al.*, 2012). Among these MMPs, MMP2, MMP9, MMP12 and MMP14 are the key factors responsible for stem cell mobilization and tissue remodelling in transplantation and regeneration of injured tissue (Harris *et al.*, 2010; Shirvaikar *et al.*, 2012). However, the intracellular signalling mechanisms underlying the regulation of MMP expression in ROS-mediated stem cell motility have yet to be elucidated. In addition to MMPs, the ROS signalling pathway is also closely associated with the production of ECM, its assembly and turnover (Nikitovic *et al.*, 2013; Eble and Figueiredo de Rezende, 2014). Indeed, it has been shown that H_2O_2 is essential for the induction of collagen (COL) and fibronectin (FN) in human mesangial cells (Iglesias-De La Cruz *et al.*, 2001). If we assume that ROS regulate the levels of MMP and ECM proteins and subsequently improve stem cell motility, H_2O_2 as well as downstream signalling mechanisms could be promising targets for stem cell therapy. Thus, it is important to determine the role of H_2O_2 in the regulation of MMP and ECM protein expression when considering stem cells for use in regeneration strategies.

Human umbilical cord blood-derived mesenchymal stem cells (UCB-MSCs) are considered to be one of the most abundant sources of non-ESCs (Qiao *et al.*, 2008). UCB-MSCs are known to have self-renewal capacity, have relatively low immunogenicity and can differentiate into multiple cell types (Le Blanc *et al.*, 2003; Yang *et al.*, 2004; Qiao *et al.*, 2008). Thus, the therapeutic potential of UCB-MSCs has been evaluated in many pathophysiological animal models (Jeong *et al.*, 2005; Wakitani *et al.*, 2007; Sensebe *et al.*, 2010). Although several studies have described the results obtained when MSCs have been applied clinically, transplanted for the regeneration of injured tissue (Wakitani *et al.*, 2007), one of the most interesting questions is how microenvironmental factors in the wounded area affect these transplanted cells and alter their behaviour. Therefore, we have investigated the role of H_2O_2, and associated signalling pathways, in promoting the motility of UCB-MSCs.

Methods

Materials

UCB-MSCs were kindly provided by Medipost Co. (Seoul, Korea), and were isolated and expanded as reported previously (Yang *et al.*, 2004). These cells have been characterized to express CD105 (99.6%) and CD73 (96.3%), but not CD34 (0.1%), CD45 (0.2%) and CD14 (0.1%). They were positive for human leukocyte antigens (HLA)–AB gene but generally not for HLA-DR gene (Yang *et al.*, 2004). The UCB-MSCs have the ability to differentiate into various cell types such as osteoblasts, chondrocytes and adipocytes upon *in vitro* induction with the appropriate osteogenic, chondrogenic and adipogenic differentiation stimuli (Yang *et al.*, 2004). In the present study, all the experiments were carried out with cells from the seventh passages. Mouse ESCs were obtained from the American Type Culture Collection (ES-E14TG2a; Manassas, VA, USA). FBS was purchased from BioWhittaker, Inc. (Walkersville, MO, USA). Phospho-ERK1/2, ERK, phospho-JNK/SAPK, JNK/SAPK, phospho-p-38 MAPK and p38 MAPK antibodies were obtained from the R&D Systems (Minneapolis, MN, USA). A23187, bisindolylmaleimide I, H_2O_2, lithium chloride (LiCl), PD98059, SB203580, staurosporine, MMP408, mitomycin C and vitamin C were obtained from Sigma Chemical

Company (St. Louis, MO, USA). SN 50 was purchased from Calbiochem (La Jolla, CA, USA). Bay11-7082 was purchased from Biomol International, LP (Plymouth Meeting, PA, USA). β-Actin, β-catenin, COL-1A, COL-3A, COL-5A, FN, glycogen synthase kinase-3β (GSK-3β), lamin A/C, NF-κB, MMP9, MMP12, MMP16, pan-cadherin, phospho-GSK-3β, phospho-NF-κB (p65), PKC, PKCα, PKCε, PKCθ and PKCζ antibodies were purchased from Santa Cruz Biotechnology (Santa Cruz, CA, USA). Phospho-PKC antibody was purchased from Cell Signaling (Beverly, MA, USA). HRP-conjugated goat anti-rabbit and goat anti-mouse IgG were purchased from Jackson Immunoresearch (West Grove, PA, USA). All other reagents were of the highest purity commercially available.

Culture of human UCB-MSCs

Human UCB-MSCs were cultured without a feeder layer in α-minimum essential medium (α-MEM; Thermo, Waltham, MA, USA), 1% penicillin/streptomycin and 10% FBS. For each experiment, cells were grown in 6- and 12-well plates, and in 35, 60 or 100 mm diameter culture dishes in an incubator maintained at 37°C with 5% CO_2. The medium was replaced with serum-free α-MEM at least 24 h before the experiments. Following the incubation, the cells were washed twice with PBS and then maintained in a serum-free α-MEM including all supplements and indicated agents.

In vitro *wound-healing assay*

Human UCB-MSCs were seeded at 4×10^4 cells in both silicone reservoirs, which were separated by a 500 μm thick wall (Ibidi, Martinsried, Germany) (Chieng-Yane *et al.*, 2011) and incubated until the cell reached around 100% confluence in the serum-containing medium. After incubation in serum-free medium (serum starvation) for 24 h, the silicone reservoirs were removed with sterile forceps to create a wound field. The cells were incubated for an additional 24 h in H_2O_2 and visualized with an Olympus FluoView™ 300 confocal microscope with 100× objective.

Oirs™ cell migration assay

Human UCB-MSCs were seeded at 3×10^2 cells 100 μL^{-1} in an Oirs well (Platypus Technologies, Fitchburg, WI, USA) and incubated for 24 h to allow cell adhesion to occur. Inserts were carefully removed when the cell reached around 70% confluence, and the wells were gently washed with culture medium. Cells were then incubated with H_2O_2 and serum-free medium. Cell motility was observed microscopically after 24 h. Cell populations in end point assays were stained with 5 μM calcein AM for 30 min. Migrated cells were quantified by measuring the fluorescence signals using a microplate reader at excitation and emission wavelengths of 485 and 515 nm respectively (Park and Han, 2009).

Live cell imaging microscopy

Cells were placed in temperature/CO_2 control chambers (Tokai Hit, Heidelberg, Germany) attached to an Olympus IX81-ZDC zero-drift microscope (Olympus, Center Valley, PA, USA). Images were collected for 0–24 h at 5 min intervals, using a Cascade 512B camera (Roper Scientific, Trenton, NJ, USA) operated by the multidimensional acquisition package of MetaMorph v. 7.01 software (Molecular Devices, Sunnyvale, CA, USA).

Intracellular ROS detection

CM-H2DCFDA (DCF-DA) was used to detect the generation of ROS. To quantify the intracellular ROS levels, the cells treated with 10 mM DCF-DA were washed twice with ice-cold PBS and then scraped. One hundred microlitres of cell suspension was loaded into a 96-well plate and examined using a luminometer (Victor3; Perkin-Elmer, Waltham, MA, USA) and a fluorescent plate reader at excitation and emission wavelengths of 485 and 535 nm respectively.

Cell proliferation

Cells seeded at a density of 4×10^5 cells per well were synchronized by incubation in serum-free medium for 36 h. Cells were then treated with 1 μM H_2O_2 for 48 h, and the number of cells counted daily using a haemocytometer.

[^{3}H]-thymidine incorporation

The [^{3}H]-thymidine incorporation experiments were performed as previously described by Brett *et al.* (1993). Briefly, UCB-MSCs were synchronized by incubation in serum-free medium for 36 h and then exposed to 1 μM H_2O_2 for 24 h. After the incubation period, 1 μCi of [methyl-^{3}H]-thymidine (specific activity: 74 GBq·mmol^{-1}, 2.0 Ci·mmol^{-1}; Amersham Biosciences, Buckinghamshire, UK) was added to the cultures for 1 h at 37°C. Cellular [^{3}H]-thymidine uptake was quantified by liquid scintillation counting of harvested cellular material (Wallac, Turku, Finland). All values were converted from absolute counts to percentages of control and reported as mean ± SEM of triplicate experiments.

RNA isolation and reverse transcription-PCR (RT-PCR)

Total RNA was extracted using the RNeasy Plus Mini Kit (Qiagen, Valencia, CA, USA). RT was carried out with 3 μg of RNA using a Maxime RT premix kit (iNtRON Biotechnology, Sungnam, Korea). The cDNA (5 μL) for the *MMP* family was amplified using the primers described in Supporting Information Table S1.

Real-time PCR

The real-time quantification of the *MMP* family was performed using a Rotor-Gene 6000 real-time thermal cycling system (Corbett Research, Mortlake, New South Wales, Australia) with a QuantiMix SYBR Kit (PhileKorea Technology, Daejeon, Korea) according to the manufacturer's instructions with minor modifications as previously described (Yun *et al.*, 2012). β-Actin was used as an endogenous control.

Confocal microscopy

UCB-MSCs were washed twice with cold PBS, fixed in 4% paraformaldehyde in PBS for 10 min at room temperature, permeabilized in 0.1% Triton X-100 (Sigma-Aldrich, St. Louis, MO, USA) in PBS for 5 min and blocked in PBS containing 10% BSA (Sigma-Aldrich) for 30 min at room temperature. Cells were then stained with primary antibody overnight at 4°C. Following three washes with PBS, the cells were incubated with Alexa Fluor 488-conjugated goat anti-rabbit/mouse IgM (Invitrogen Co., Carlsbad, CA, USA) or phalloidin (Invitrogen Co.), counterstained with PI in PBS containing 1% (v/v) BSA

and washed three times for 10 min each with PBS. Samples were mounted on slides and visualized with an Olympus FluoView 300 confocal microscope with 400× objective.

siRNA transfection

Cells were grown until 75% of the surface of the plate was covered after which they were transfected for 24 h with either a siRNA specific for *MMP12* (200 pmol·L^{-1}; GenePharma, Shanghai, China) or a *non-targeting* siRNA as a negative control (200 pmol·L^{-1}; GenePharma) with Hyperfectamine (Qiagen) according to the manufacturer's instructions. The sequences used are described in Supporting Information Table S2 and determined *MMP12* siRNA efficacy and effect of basal level respectively (Supporting Information Fig. S1).

Western blot analysis and subcellular fractionation

Western blotting was performed as previously described (Kurien and Scofield, 2006) with minor modifications (Yun *et al.*, 2012). The subcellular fractionation method for the isolation of membrane, cytosolic and nuclear proteins was as previously reported (Cox and Emili, 2006).

Immunoprecipitation

Phosphorylation of PKCα was analysed by immunoprecipitation and Western blotting. Cells were lysed with lysis buffer (1% Triton X-100 in 50 mM Tris-HCl pH 7.4 containing 150 mM NaCl, 5 mM EDTA, 2 mM Na_3VO_4, 2.5 mM Na_4PO_7, 100 mM NaF, 200 nM microcystin lysine–arginine and protease inhibitors). Cell lysates (400 μg) were mixed with anti-PKCα. The samples were mixed with protein A/G PLUS-agarose immunoprecipitation reagent (Pierce, Rockford, IL, USA) and then incubated for 12 h. The beads were washed four times, and the bound proteins were released from the beads by boiling in SDS-PAGE sample buffer for 5 min. Samples were analysed by Western blotting with p-PKC antibody.

Trichloroacetic acid (TCA) precipitation

Filtered culture supernatants were mixed with TCA to a final concentration of 30% (w/v) and were incubated on ice for 30 min or stirred overnight at 4°C. Samples were centrifuged at 10 000× *g* for 20 min. Pellets were washed with ice-cold 96% ethanol (v/v) and acetone, and were air dried.

Measurement of calcium influx

Changes in intracellular calcium concentrations were monitored using Fluo-3-AM as previously reported (Kawano *et al.*, 2002). Fluorescence was excited at 488 nm, and the emitted light was observed at 515 nm. All analyses of calcium influx were processed in a single cell, and the results are expressed as the fluorescent intensity.

Mouse skin wound-healing model

Eight-week-old female ICR mice were used. The animal experiments were carried approved by the Institutional Animal Care and Use Committee of Seoul National University (SNU-140123-6) and were in accordance with the NIH Guide for the Care and Use of Laboratory Animals. In addition, six authors were doctors of veterinary medicine with licenses granted from the Ministry of Agriculture and Forestry of Republic of Korea. All studies involving animals are reported in accordance with the ARRIVE guidelines for reporting experiments involving animals (Kilkenny *et al.*, 2010; McGrath *et al.*, 2010). Mice were anaesthetized using a 2:1 mixture of zoletil™ (20 mg·kg^{-1}; Virbac Laboratories, Carros, France) and xylazine HCl (10 mg·kg^{-1}, Rompun®; Bayer, Leverkusen, Germany) to assess the depth of anaesthesia in mice. Mouse skin wounding and stem cell implantation were performed as described previously (Lee *et al.*, 2011; Kishibe *et al.*, 2012). Briefly, after their backs had been shaved and treated with an organic iodine solution, a circular full-thickness wound was surgically created using an 8 mm diameter sterile biopsy punch. Experimental animals were divided into four groups: wild-type mice that received vehicle (group 1, $n = 7$) or H_2O_2 (group 2, $n = 7$) without UCB-MSCs; and a topical UCB-MSCs transplantation group that were given UCB-MSCs treated with vehicle (group 3, $n = 7$) or H_2O_2 (group 4, $n = 7$). We injected 1×10^6 UCB-MSCs in 70 μL of PBS into the dermis at two sites around the wound. We also applied 0.3×10^6 UCB-MSCs topically in 30 μL of growth factor-reduced Matrigel (BD Biosciences, Franklin Lakes, NJ, USA) onto the wound bed. After that, the wounds were dressed with Tegaderm (3M, London, Canada). Images of the wounds were obtained on days 0, 4, 7 and 9 with a digital camera system (D50; Nikon, Tokyo, Japan) at the same camera/subject distance (30 cm). The sizes of wound closure were determined by measuring wound resealing from the images captured at the wounded sites. At day 9, the wound tissues were embedded in O.C.T. compound (Sakura Finetek, Torrance, CA, USA), stored at −70°C, samples of 6 μm thick frozen sections were cut using a cryosectioning machine, and mounted on SuperFrost Plus Slides (Thermo Fisher Scientific, Rockford, IL, USA) for haematoxylin and eosin staining.

Statistical analysis

Results are expressed as means ± SEM. All experiments were analysed using ANOVA, followed in some cases by a comparison of treatment means with the control using the Bonferroni–Dunn test. Differences were considered statistically significant at $P < 0.05$.

Results

Effects of H_2O_2 on human UCB-MSCs motility

Cells were exposed to various concentrations (0–1000 μM) of H_2O_2 to examine the role of ROS in UCB-MSCs motility. As shown in Figure 1A, H_2O_2 significantly increased cell motility at 0.1 and 1 μM for 24 h, whereas higher concentrations of H_2O_2 decreased motility. In addition, an increase in cell motility was observed after 8 h incubation with 1 μM H_2O_2 (Figure 1B). We further explored the ability of 1 μM H_2O_2 to induce cell motility using an *in vitro* wound-healing migration assay. In contrast to the control, 1 μM H_2O_2 evoked substantial migration of cells into the denuded area (Figure 1C). The results in live cell imaging microscopy showed that H_2O_2 induced significant translocation of cell bodies into the denuded area for wound healing (Supporting Information Fig. S2, Supporting Information Video S1 and

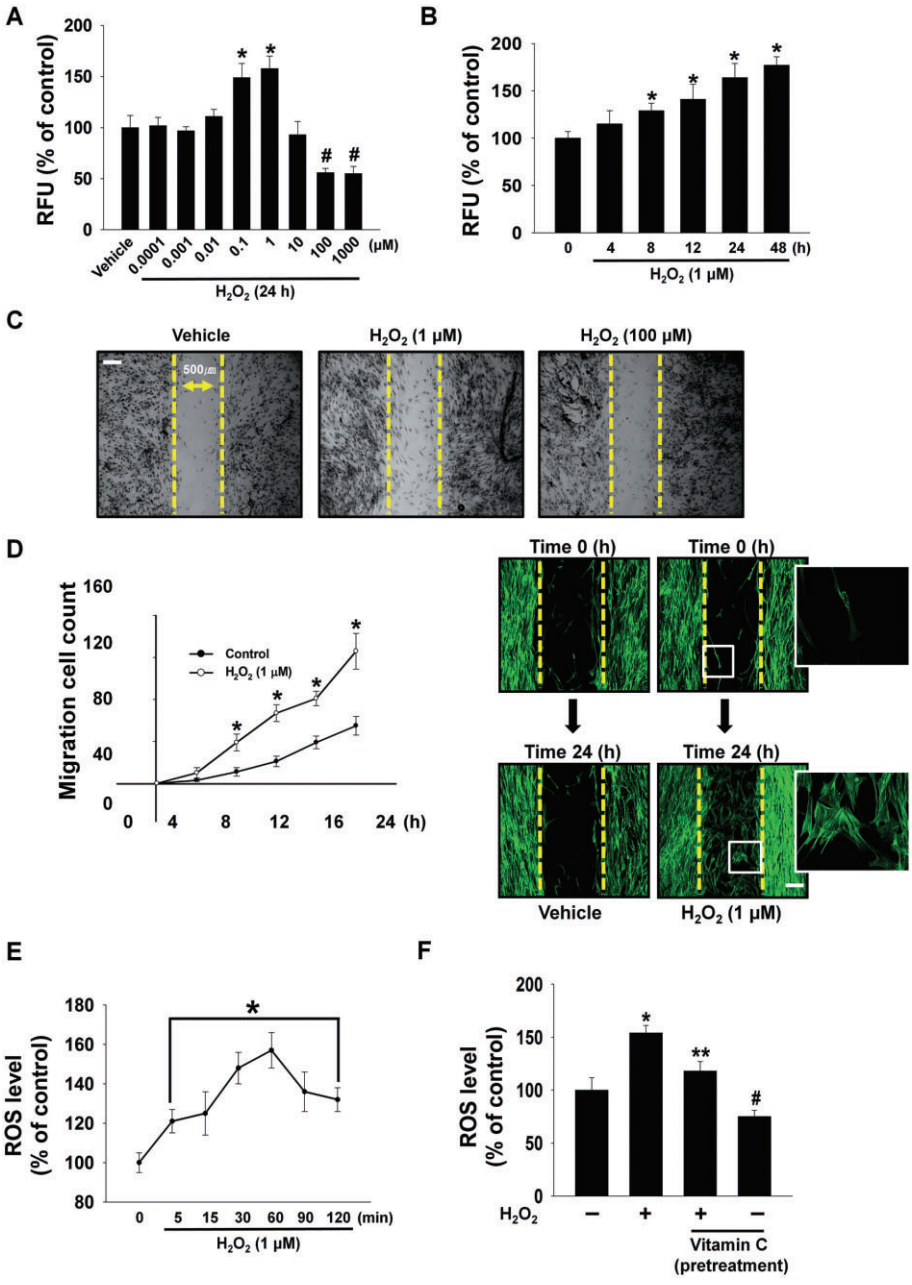

Figure 1

Effects of H_2O_2 on human UCB-MSCs migration and ROS generation. (A) Dose- responses of H_2O_2 for 24 h in Oris™ cell migration assay are shown. Data represent means ± SEM of five independent experiments with triplicate dishes. *$P < 0.05$ versus vehicle. #$P < 0.05$ versus vehicle. (B) Time responses of 1 μM H_2O_2 in Oris cell migration assay are shown. $n = 4$, *$P < 0.01$ versus 0 h. (C) *In vitro* wound healing of UCB-MSCs treated with 1 or 100 μM H_2O_2 is shown. $n = 10$. Scale bars represent 200 μm (magnification, ×100). (D) H_2O_2 (1 μM)-induced cell migration was determined by time lapse imaging experiment for 24 h. The line graph in left panel denotes the number of cells determined using the multidimensional acquisition package of MetaMorph v. 7.01 software (Molecular Devices). [Moving images can be viewed in the online issue, which is available at Supporting Information Video S1 and S2]. After live cell imaging, cell migration was confirmed by staining filamentous (F)-actin with Alexa Fluor 488-conjugated phalloidin (right panel). Scale bars represent 200 μm (magnification, ×100). $n = 5$. *$P < 0.05$ versus control. (E) ROS levels in cells treated with 1 μM H_2O_2 treatment are shown. Data represent means ± SEM of five independent experiments with triplicate dishes. *$P < 0.05$ versus 0 h. (F) ROS levels in cells treated with vitamin C are shown. Cells were pretreated with 1 mM vitamin C for 30 min and then exposed to 1 μM H_2O_2 for 30 min. Data represent means ± SEM of five independent experiments with triplicate dishes. *$P < 0.05$ versus vehicle, #$P < 0.05$ versus vehicle, **$P < 0.05$ versus H_2O_2 alone. F-actin, filamentous actin; RFU, relative fluorescence units.

S2). Consistent with our findings from a typical set of time-lapse experiments, H_2O_2 increased the number of cells that moved into the wounded area (Figure 1D, left panel). After live cell imaging, the filamentous (F)-actin structure was visualized by staining UCB-MSCs with Alexa Fluor 488-conjugated phalloidin (Figure 1D, right panel). We further confirmed that 1 μM H_2O_2 entered the migrating cells. A significant increase in ROS appeared in the cells after a 5 min incubation with 1 μM H_2O_2 (Figure 1E); this was inhibited by vitamin C (Figure 1F). It is noted that UCB-MSCs were pretreated with vitamin C to eliminate the possibility of endogenous H_2O_2 contributing to the ROS level. In order to eliminate the possibility that the migration is related to the proliferation of the cells, we pretreated the cells with mitomycin C, a potent DNA cross-linker that inhibits cell proliferation, in the presence or absence of H_2O_2. However, H_2O_2-induced wound closure was not affected by the mitomycin C treatment (Supporting Information Fig. S3). This indicates that the effect of H_2O_2 on cell migration is independent of cell proliferation. To confirm that H_2O_2 does not affect cell proliferation, we further investigated whether H_2O_2 has an effect on the levels of DNA synthesis and cell number using [^{3}H]-thymidine incorporation (Supporting Information Fig. S4) and a cell counting assay (Supporting Information Table S3) respectively. However, 1 μM H_2O_2 had no significant effects on the level of DNA synthesis and cell number compared with the control.

Effect of H_2O_2 on activation of PKC and ERK/p38 MAPK

ROS play an important role as signal messengers in promoting cell motility through activation of PKC and MAPKs (Wu *et al.*, 2008), therefore, we examined whether H_2O_2 induced phosphorylation of PKC. H_2O_2 significantly increase the phosphorylation of PKC at 30 min (Figure 2A). In addition, translocation of PKCα from the cytosol to the membrane compartment was observed in cells treated with H_2O_2 for 60 min (Figure 2B). The translocation of PKCα showed a corresponding pattern as assessed by immunofluorescence staining (Figure 2C). In addition, we found that p-PKC co-immunoprecipitated with PKCα, and importantly, the specific phosphorylation of PKCα was enhanced by H_2O_2 treatment (Supporting Information Fig. S5). These data suggest a functional role of PKCα in regulating H_2O_2-mediated cell motility. Pretreatment with vitamin C reduced H_2O_2-induced PKC phosphorylation (Figure 2D). H_2O_2 also enhanced calcium influx, which was blocked by vitamin C (Figure 2E). We further investigated the involvement of MAPK activation in the UCB-MSCs motility elicited by H_2O_2. H_2O_2 increased the phosphorylation of ERK and p38 MAPK for 15–120 min (Figure 2F), but did not affect JNK/SAPK phosphorylation, and its effect was inhibited by PKC inhibitors, bisindolylmaleimide I and staurosporine (Figure 2G). These data provide the important evidence that PKCα-mediated ERK/p38 MAPK phosphorylation is required for the H_2O_2-induced increase in UCB-MSCs motility.

Involvement NF-kB phosphorylation and GSK-3β/β-catenin

We further examined the role of H_2O_2 in activation of NF-κB and β-catenin, as an important ROS signalling intermediates (Kumar *et al.*, 2007). As shown in Figure 3A, H_2O_2 increased NF-κB phosphorylation between 15 and 90 min, and also increased GSK-3β phosphorylation and β-catenin expression between 30 and 120 min. In addition, pretreatment with the ERK inhibitor PD98059 and p38 MAPK inhibitor SB203580 significantly blocked the phosphorylation of NF-κB induced by H_2O_2. However, the GSK-3β phosphorylation induced by H_2O_2 was only inhibited by PD98059, but not SB203580 (Figure 3B). A nuclear and non-nuclear protein fractionation assay showed that H_2O_2 and the GSK-3β inhibitor, LiCl increased the accumulation of β-catenin in the nuclear fractions. The enrichment of the non-nuclear or nuclear fraction was validated by the apparent increase in the membrane marker pan-cadherin and the nuclear marker lamin A/C (Figure 3C). However, LiCl did not affect NF-κB phosphorylation (Figure 3C). The nuclear accumulations of β-catenin and p-NF-κB induced by either H_2O_2 or LiCl treatment were further confirmed by immunofluorescence staining (Figure 3D and E).

Role of H_2O_2 in the degradation of COL-5 and FN via MMP12

Because changes in MMP expression are associated with the increase in cell motility, we first determined the existence of MMP isotypes in human UCB-MSCs. UCB-MSCs exhibited various kinds of MMPs mRNA amplicons, such as *MMP1*, *2*, *11*, *12*, *14*, *16*, *17* and *19* (Figure 4A). However, H_2O_2 selectively augmented the *MMP12* and *MMP16* mRNA expression levels (Figure 4B). Interestingly, H_2O_2 increased MMP12 protein levels in lysates and in cell culture supernatants, but did not increase those of MMP16 (Figure 4C). Furthermore, increased immunofluorescence staining of MMP12 was observed in the cells treated with 1 μM H_2O_2 for 12 h (Figure 4D). We then determined whether the MMP12 protein level is regulated by the activation of NF-κB and β-catenin. Pretreatment with NF-κB inhibitors (SN 50 or Bay 11-7082) significantly inhibited H_2O_2-induced increase in MMP12 protein level (Figure 4E). The GSK-3β inhibitor, LiCl, also increased the MMP12 protein level in lysates and in cell culture supernatants in a similar manner to H_2O_2 (Figure 4F). These results suggest that H_2O_2 uniquely regulates the level of MMP12 by activation of NF-κB and β-catenin and thus promotes UCB-MSCs motility.

To confirm this functional role of MMP12, we further determined whether H_2O_2 regulates degradation of ECM proteins, such as COLs and FN. As shown in Figure 5A, H_2O_2 decreased COL-5 and FN concentration in cell culture supernatants without changing COL-5 or FN protein level in cell lysates, but it did not affect COL-3/-5 levels. However, neither the MMP12 inhibitor, MMP408 nor *MMP12* siRNA significantly inhibited COL-5 and FN degradation in H_2O_2-treated UCB-MSCs (Figure 5B and C). The degradations of COL-5 and FN induced by H_2O_2 were further confirmed in UCB-MSCs transfected with the *nt* siRNA (Supporting Information Fig. S6).

Next, we examined the effects of H_2O_2 and its related signalling molecules on the motility of human UCB-MSCs. These UCB-MSCs were pretreated with vitamin C; PKC inhibitors bisindolylmaleimide I and staurosporine; ERK inhibitor PD 98059; p38 MAPK inhibitor SB294002; NF-κB inhibitors SN50 and Bay 11-7082; MMP12 inhibitor

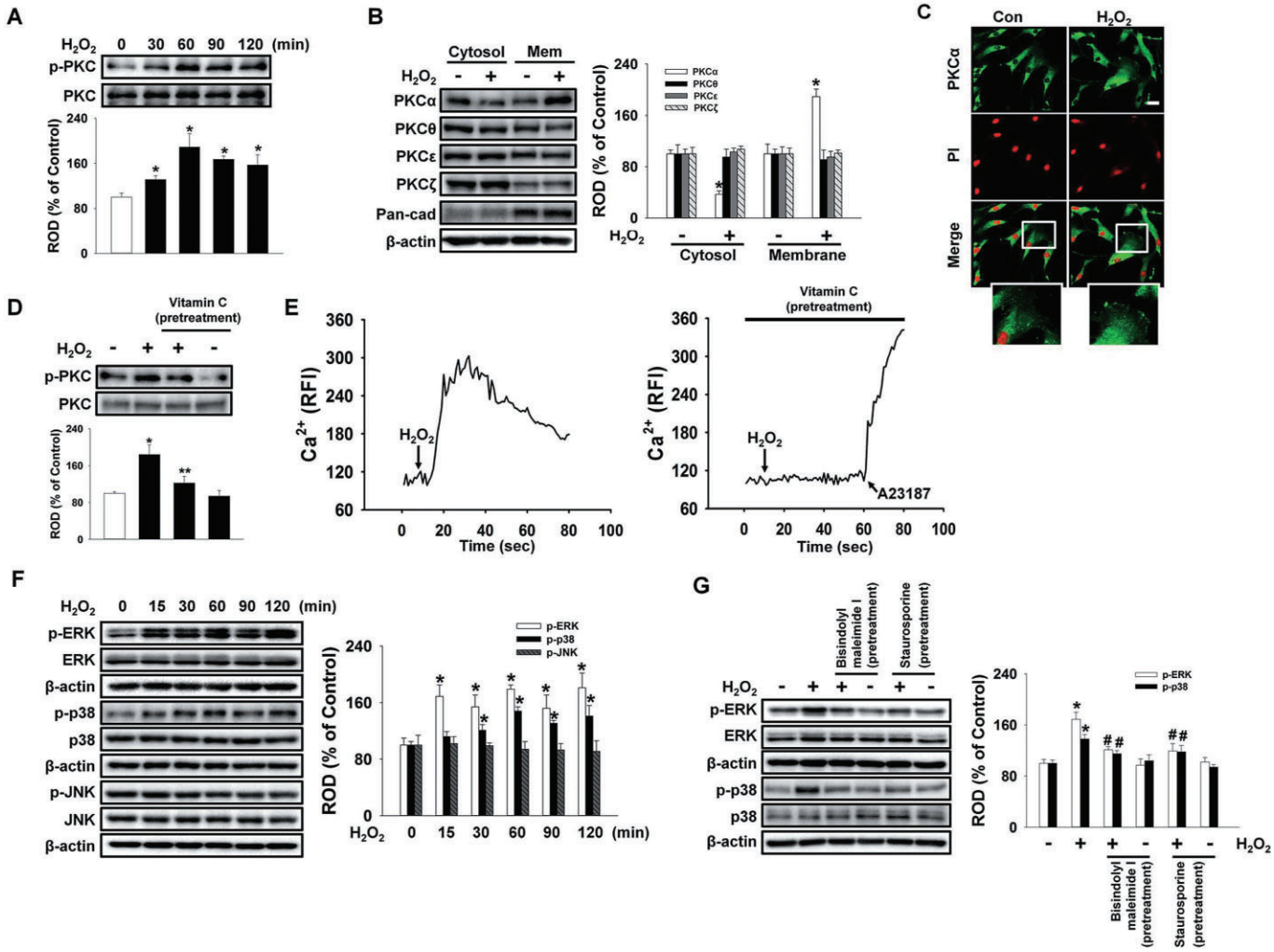

Figure 2

Involvement of PKC and MAPK activation. (A) Phosphorylation of PKC in cells treated with H_2O_2 is shown. (B) Membrane translocation of PKC isoforms in cells treated with H_2O_2 (1 μM) for 60 min was determined by Western blot analysis. (C) Membrane translocation of PKCα (green) was determined by confocal microscopy using immunofluorescence staining. Propidium iodide (PI) was used for nuclear counterstaining (red). Scale bars, 100 μm (magnification, ×400). $n = 3$. (D) Phosphorylation of PKC in cells treated with vitamin C is shown. Cells were pretreated with 1 mM of vitamin C for 30 min and then exposed to 1 μM H_2O_2 for 60 min. (E) Ca^{2+} influx in cells treated with 1 μM H_2O_2 in the absence (left panel) and presence (right panel) of vitamin C was determined by confocal microscopy using Fluo-3/AM staining. The results were expressed as relative fluorescence intensity (RFI, F/F0%, arbitrary unit). (F) Phosphorylation of ERK, p38 and JNK in cells treated with H_2O_2 was determined. (G) Phosphorylation of ERK and p38 is shown. Cells were pretreated with bisindolylmaleimide I and staurosporine (10 μM) for 30 min and then exposed to 1 μM H_2O_2 for 60 min. (A, B, D, F and G) Error bars represent the mean ± SEM of four independent experiments for each condition determined by densitometry relative to total PKC, total ERK, total p38, total JNK or β-actin. $^*P < 0.05$ versus vehicle, $^{\#}P < 0.05$ versus H_2O_2 alone. ROD, relative optical density.

MMP408, *MMP12* siRNA and *nt* siRNA; and then exposed to H_2O_2 or the GSK-3β inhibitor LiCl under normal cell culture conditions. The increased cell motility induced by H_2O_2 treatment was inhibited by signal pathway-related molecule siRNAs or inhibitors, but not by LiCl (Figure 6A and B). To confirm the functional role of H_2O_2 in promoting UCB-MSCs motility, we further investigated the effect of UCB-MSCs treated with H_2O_2 on skin wound healing in mice. There are no significant differences between wound sizes of mice treated with vehicle or H_2O_2 alone, although spontaneous wound healings were observed from day 7 (Figure 6C). On days 7 and 9, however, wound healing was significantly accelerated in the group of mice that received UCB-MSCs treated with H_2O_2, compared with the UCB-MSCs + vehicle group. It is noted that topical application of UCB-MSCs also enhanced wound healing, compared with the mice treated with the vehicle from day 7. Histological examination at day 9 showed that the wound bed was still not completely covered with epidermis or a cornified layer in mice treated with vehicle or H_2O_2 alone (Figure 6D). However, the topical UCB-MSCs transplantation groups showed an increased re-epithelialization from the mechanical skin wound, but the

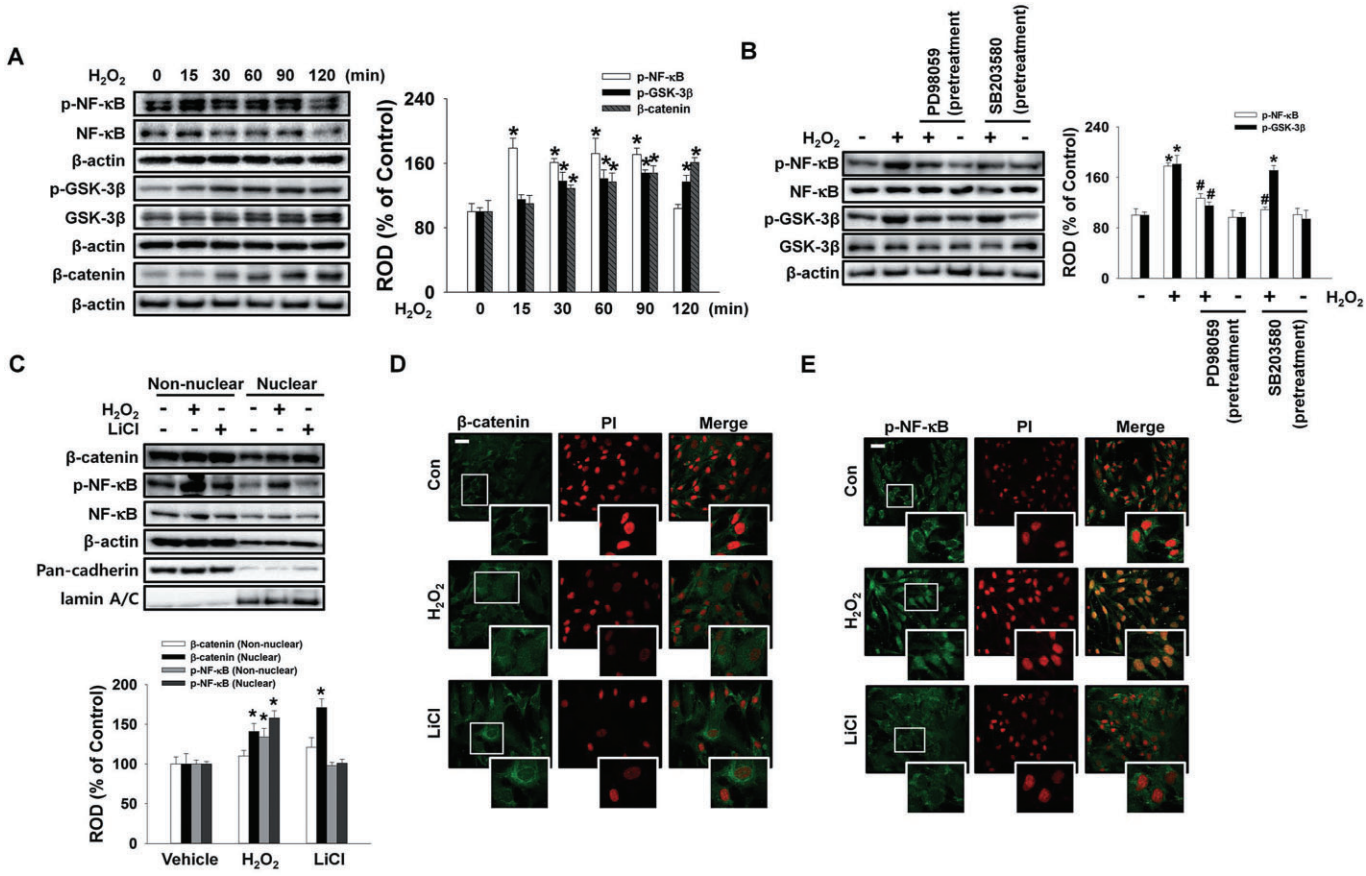

Figure 3

Effects of H_2O_2 on NF-κB, GSK-3β phosphorylation and β-catenin translocation. (A) Phosphorylation of NF-κB and GSK-3β, and expression of β-catenin were determined by Western blot analysis. (B) Phosphorylation of NF-κB and GSK-3β is shown. Cells were pretreated with PD98059 (10 μM) and SB203580 (1 μM) for 30 min and then exposed to 1 μM H_2O_2 for 90 min. (C) Nuclear translocation of β-catenin and phospho-NF-κB in cells treated with H_2O_2 (1 μM) and LiCl (10 mM) for 90 min was determined by Western blot analysis. Pan-cadherin and lamin A/C were used as internal control for non-nuclear and nuclear fractions respectively. Nuclear translocations of β-catenin (D, green) and phospho-NF-κB (E, green) were determined by confocal microscopy using immunofluorescence staining. Propidium iodide (PI) was used for nuclear counterstaining (red). Scale bars, 100 μm (magnification, ×400). $n = 3$. (A–C) Error bars represent the mean ± SEM of five independent experiments for each condition determined from densitometry relative to total NF-κB, total GSK-3β or β-actin. $^*P < 0.05$ versus vehicle, $^{\#}P < 0.05$ versus H_2O_2 alone. ROD, relative optical density.

epidermis and cornified layer of wounds of the mice group that received UCB-MSCs treated with H_2O_2 was almost completely restored.

Discussion

Our data demonstrated that H_2O_2 regulates human UCB-MSCs motility by facilitating MMP12-mediated COL-5 and FN degradation through the distinct activation of the ERK/p38MAPK/NF-κB and ERK/GSK-3β/β-catenin pathways. Thus, our findings suggest that H_2O_2 has good therapeutic potential to improve wound recovery and tissue regeneration processes. We first showed that H_2O_2 has the ability to induce cell motility at a low dose (0.1–1 μM), but at ≥100 μM H_2O_2 tended to reduce cell motility. Although these opposite effects of H_2O_2 seem to be mediated by different signalling pathways (Goldkorn *et al.*, 1998; Lee *et al.*, 2009; Xiao *et al.*, 2009), many previous reports have shown that H_2O_2 at low doses (<100 μM) induces the proliferation, survival and differentiation of various stem cells (Lee *et al.*, 2009; Xiao *et al.*, 2009), whereas at high doses (>100 μM), H_2O_2 induces programmed cell death (Goldkorn *et al.*, 1998). These findings indicate that stem cell fates are dependent on H_2O_2 concentrations. It was shown that wound-induced extracellular H_2O_2 reached concentrations of 0.5–100 μM near the wound margin, based on published calibrations of HyPer in tissue cultures and murine wound fluid samples (Niethammer *et al.*, 2009). Hence, the present results suggest that the functional roles of H_2O_2 at 0.1–1 μM are physiologically relevant in the stimulation of stem cell motility via ROS generation. These results further indicate that an appropriate concentration of H_2O_2 is critical for stem cell transplantation and stem cell homing.

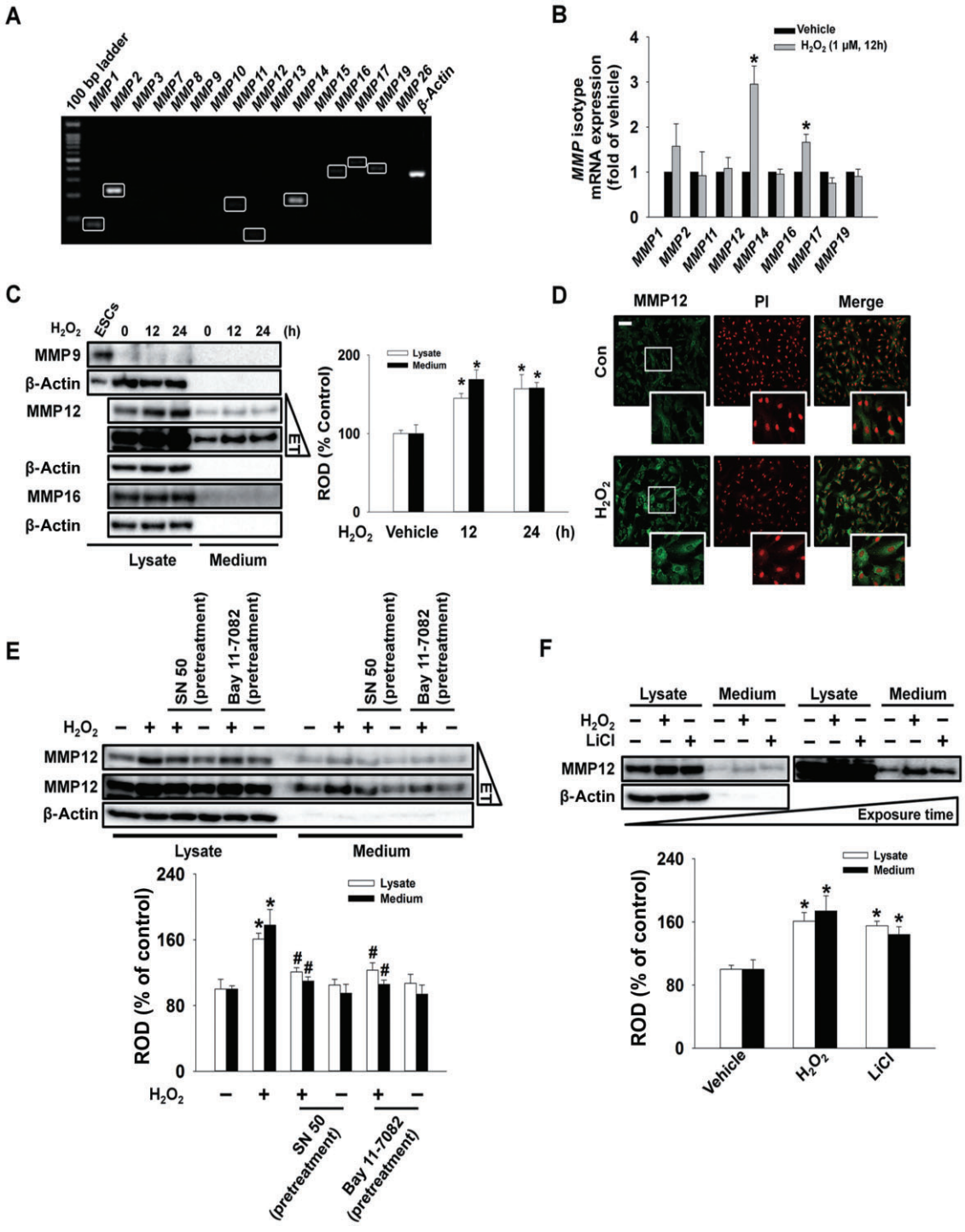

Figure 4

Effect of H_2O_2 on MMP12 expression and secretion. (A) Expression of *MMP*s mRNA in UCB-MSCs is shown. $n = 5$. (B) Expression of *MMP*s mRNA in cell treated with 1 μM H_2O_2 for 12 h was determined by real-time PCR. Data (means ± SEM) are from five independent experiments in triplicate. *$P < 0.01$ versus vehicle. (C) Protein levels of MMP9, MMP12 and MMP16 in lysates and cell culture supernatants of UCB-MSCs treated with 1 μM H_2O_2 for 12 or 24 h were determined by Western blot analysis. ESC lysate is positive control of MMP9 (Lee *et al.*, 2010b). (D) Expression of MMP12 (green) was determined by confocal microscopy using immunofluorescence staining. Propidium iodide (PI) was used for nuclear counterstaining (red). Scale bars, 100 μm (magnification, ×400). $n = 3$. (E) Protein levels of MMP12 in lysates and cell culture supernatants of UCB-MSCs are shown. Cells were pretreated with SN 50 (500 ng·mL^{-1}) and Bay 11-7082 (10 μM) for 30 min and then exposed to 1 μM H_2O_2 for 12 h. (F) Protein levels of MMP12 in lysates and cell culture supernatants of UCB-MSCs treated with H_2O_2 (1 μM) or LiCl (10 mM) for 12 h were determined by Western blot analysis. (C, E, F) Error bars represent the mean ± SEM of four independent experiments for each condition determined from densitometry relative to β-actin. *$P < 0.05$ versus vehicle, $^{\#}P < 0.05$ versus H_2O_2 alone. ET, exposure time; ROD, relative optical density.

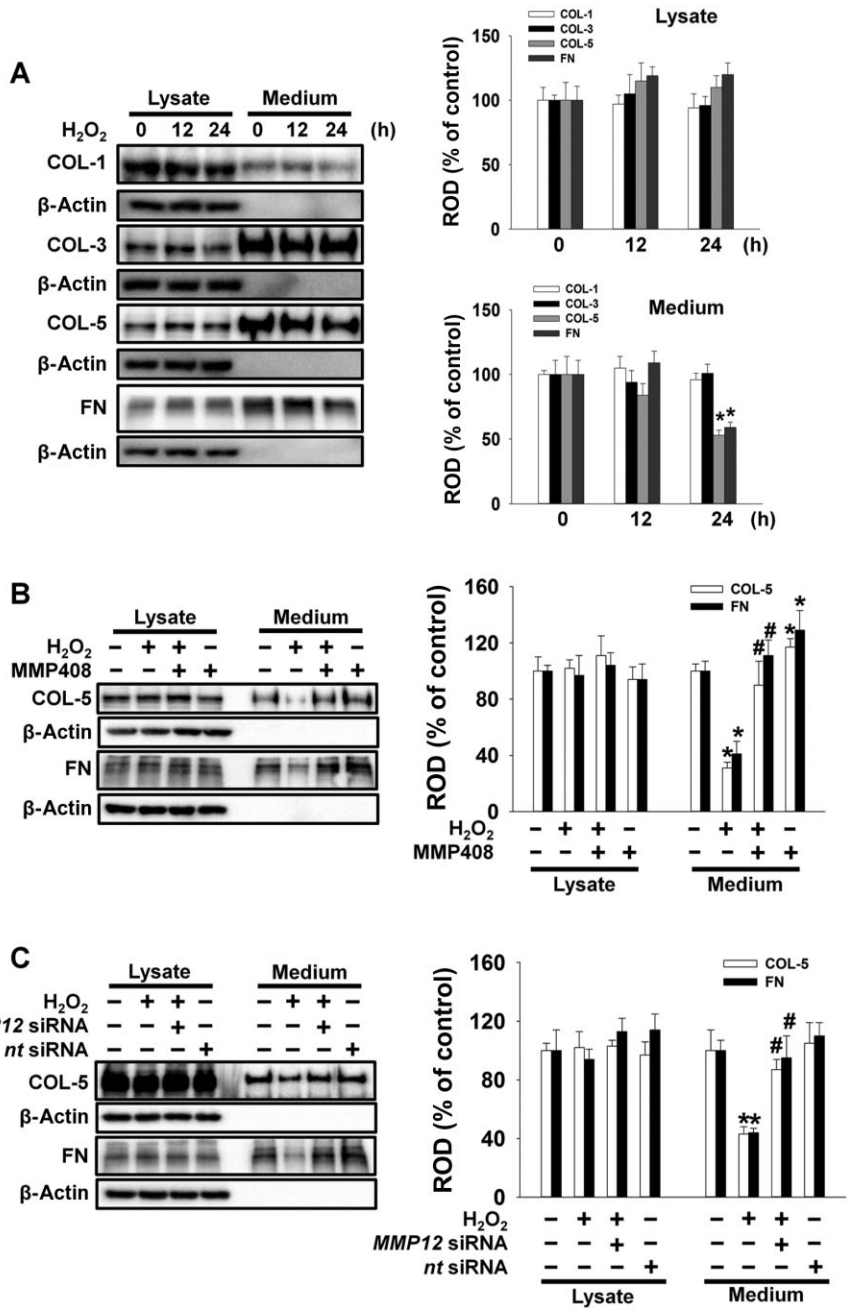

Figure 5

H_2O_2-induced MMP12 regulated ECM component protein degradation. (A) Protein levels of COL-1, COL-3, COL-5 and FN in lysates and cell culture supernatants of UCB-MSCs are shown. (B) Protein levels of COL-5 and FN in lysates and cell culture supernatants of UCB-MSCs are shown. Cells were pretreated with MMP12 inhibitor MMP408 (10 nM) for 30 min and then exposed to 1 μM H_2O_2 for 24 h. (C) Protein levels of COL-5 and FN in lysates and cell culture supernatants of UCB-MSCs transfected with *MMP12* specific siRNA (200 pmol·L^{-1}) are shown. *Non-targeting* (*nt*) control siRNA (200 pmol·L^{-1}) was used as a negative control. The knockdown efficacy of *MMP12* determined by Western blot was >70% (Supporting Information Fig. S1). (A–C) Error bars represent the mean ± SEM of five independent experiments for each condition determined from densitometry relative to β-actin. *$P < 0.05$ versus control, $^{\#}P < 0.05$ versus H_2O_2 alone. ROD, relative optical density.

We and others have suggested that multiple signalling processes such as those acting through calcium, PKC and MAPK pathways are rapidly activated in target cells through ROS, and that these pathways are linked to the discrete or allied cellular actions of H_2O_2 (Cai, 2005; Lee *et al.*, 2009). In the current study, we observed that H_2O_2 increased PKCα activation and intracellular Ca^{2+} concentration. It was shown that ROS triggered the phosphorylation of PLC, increased

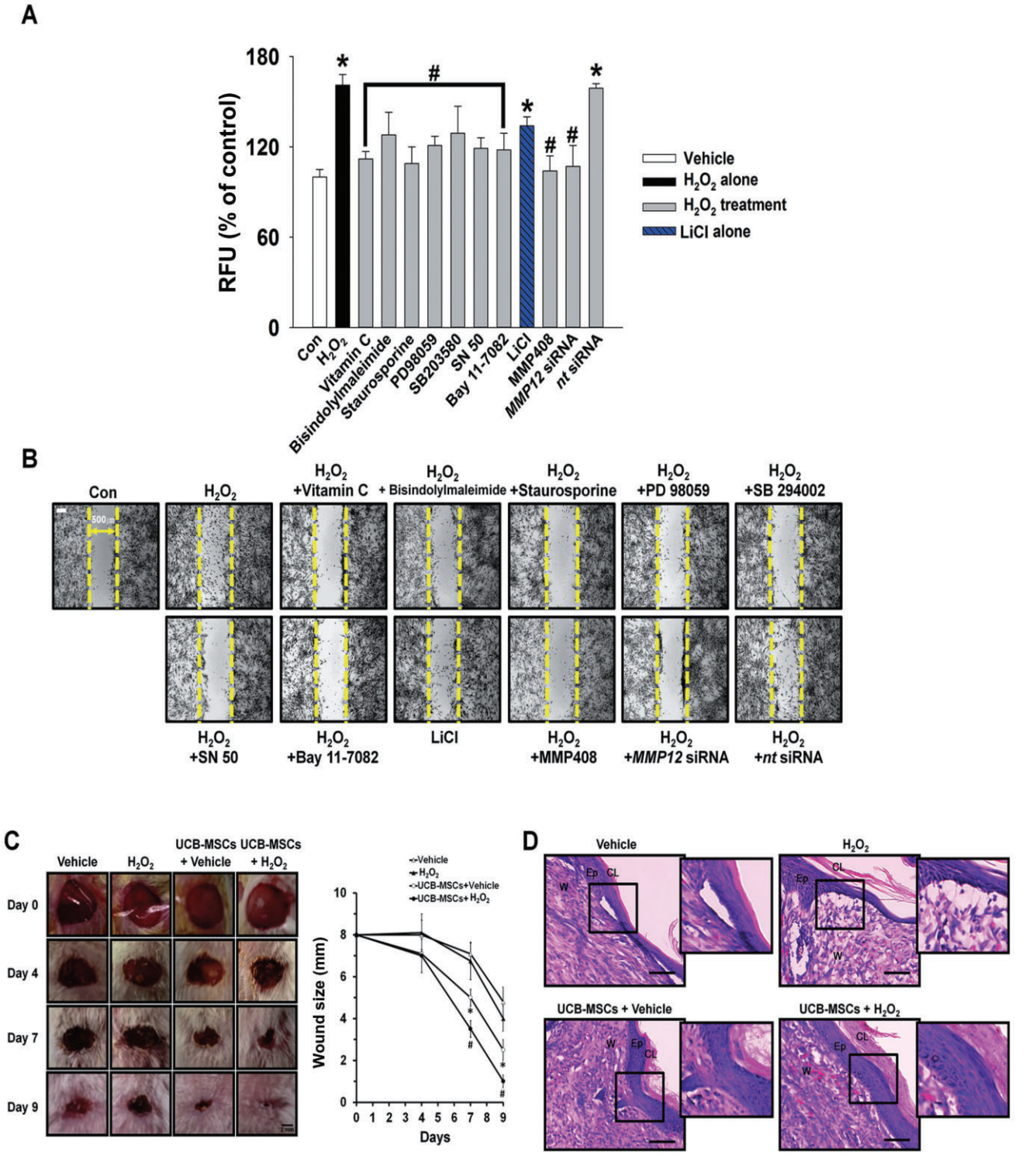

Figure 6

Role of H_2O_2 and its related signalling molecules on human UCB-MSCs motility. Cell migration was determined by Oris™ cell migration assay (A) and wound-healing assay (B). Cells were pretreated with vitamin C, bisindolylmaleimide I, staurosporine, PD98059, SB203580, SN 50, Bay 11-7082, LiCl, MMP408, *MMP-12* siRNA and *non-targeting* (*nt*) control siRNA and then exposed to 1 μM H_2O_2 for 24 h. For wound-healing assay, 10 fields per plate were examined. Scale bars represent 200 μm (magnification, ×100). (C) Representative gross images on skin wound healing at days 0, 4, 7 and 9 are shown (left panel). Mouse skin wounds were made by a 8 mm in diameter biopsy punch and treated with vehicle, H_2O_2, UCB-MSCs + vehicle and UCB-MSCs + H_2O_2 respectively. Wound sizes, quantified relative to original wound size, are shown (right panel). Error bars represent the mean ± SEM. $n = 7$. $^*P < 0.05$ versus vehicle alone, $^{\#}P < 0.05$ versus UCB-MSCs + vehicle. (D) Representative wound tissues stained with haematoxylin and eosin are shown. $n = 8$. Scale bars, 100 μm. Ep, epidermis; W, wound bed; CL, cornified layer.

$[Ca^{2+}]_i$ and consequently activated PKC in various cell types including stem cells (Bai *et al.*, 2002; Lee *et al.*, 2009; 2010a). Hence, our results are consistent with the notion that H_2O_2 plays a pivotal role in PKC activation via ROS generation. It has been shown that MAPK exists downstream of PKC and regulates many related transcription factors, including NF-κB and β-catenin, in several cell types, including human UCB-MSCs and mouse ESCs (Yun *et al.*, 2009; Yang *et al.*, 2012; Lee do *et al.*, 2013; Priyanka *et al.*, 2013). We found that H_2O_2 was able to induce ERK and p38 MAPK activation, thereby stimulating NF-κB and β-catenin activation. Regarding the role of MAPKs in NF-κB activation, earlier work showed that p38 pathway can influence NF-κB activation, at least partly, through the physical association with MAPK6 (Craig *et al.*, 2000; Yoo *et al.*, 2012). In addition, pERK1/2 was reported to have the ability to translocate into the nucleus, where it phosphorylates various substrates, such as transcriptional factors, thereby transmitting the signals received by cell surface receptors to the nucleus (Lidke *et al.*, 2010). Hence, it is conceivable that H_2O_2 has a potential role in promoting the NF-κB pathway through the activation of ERK and p38 MAPK. In addition, β-catenin is known to be released for phosphorylation by GSK-3β and for stabilization and nuclear accumulation in the canonical Wnt pathway (Atkins *et al.*, 2013). Thus, given that GSK-3β directly interacts with ERK1/2 (Ma *et al.*, 2008), it is possible that in the present study, the nuclear location of β-catenin was regulated by the preferential binding of ERK1/2 to GSK-3β and this promoted UCB-MSCs motility. Based on these results, we suggest that H_2O_2-mediated PKC activation up-regulates the NF-κB and GSK-3β-dependent signalling pathways via MAPKs and promotes UCB-MSCs motility.

Interestingly, H_2O_2 uniquely increased MMP12 protein expression of all the MMP isoforms (*MMP1*, *2*, *11*, *12*, *14*, *16*, *17* and *19* genes) in a NF-κB/β-catenin-dependent manner. This suggests that the functional role of MMPs is also influenced by the H_2O_2 signalling pathway in UCB-MSCs. Consistent with our data, previous results showed that ROS play a critical role in MMP12 expression under various experimental conditions (Lavigne and Eppihimer, 2005; Kim *et al.*, 2010), and MMP12 expression is specifically enhanced by NOX2-derived ROS production (Kim *et al.*, 2013). Hence, these findings identify MMP12 as a unique downstream mediator of the H_2O_2 signalling pathway in promoting UCB-MSCs motility. However, how NF-κB and β-catenin bind to the MMP12 promoter region remains to be elucidated. Regulation of the MMP family by extracellular stimuli including ROS has been found to be associated with ECM degradation and remodelling (Kang *et al.*, 2012; Bourboulia *et al.*, 2013). COLs and FN are known to be major substrates for MMP12, regulating the self-renewal and migration of stem cells (Magnusson and Mosher, 1998; Barnes and Farndale, 1999; Suh and Han, 2011; Park *et al.*, 2012). In the present study, COL-5 and FN degradation induced by H_2O_2 occurred in a MMP12-dependent manner. Due to the specific elastolytic activity in ECM remodelling, MMP12 expression is reportedly essential in tissue remodelling associated with emphysema in mice exposed to cigarette smoke (Hautamaki *et al.*, 1997). In addition, MMP12-null mice have been described as resistant to bleomycin-induced pulmonary fibrosis (Dunsmore *et al.*, 2001). Although MMP12 has been shown to degrade other ECM proteins, such as laminin, elastin and vitronectin in trophoblast cells; this discrepancy is probably due to differences in species, cell type or experimental conditions (Peng

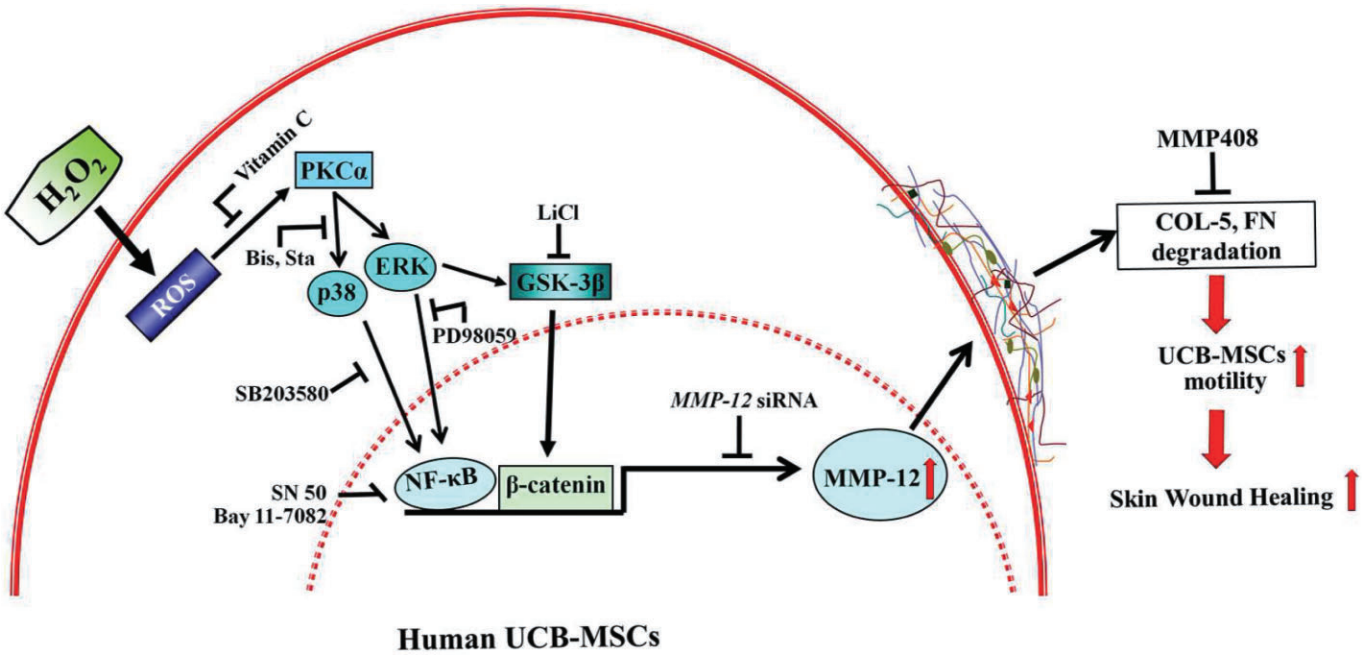

Figure 7

A hypothetical model for H_2O_2-induced signalling pathway in promoting human UCB-MSCs motility. For induction of human UCB-MSCs motility, H_2O_2 increased ERK and p38MAPK phosphorylation via PKCα activation, thereby stimulating NF-κB and GSK-3β activation that are necessary for MMP12-mediated degradation of COL-5 and FN. Bis, bisindolylmaleimide I; Sta, staurosporine.

et al., 2012); our results indicate that COL-5 and FN degradation through MMP12 expression is a critical event in promoting UCB-MSCs motility.

Overall, these findings highlight the relevance of MMP12 and ECM proteins in H_2O_2-induced enhancement of human UCB-MSCs motility (Figure 7). Similar results have been observed in bone marrow MSCs and in breast cancer stem cells (Li *et al*., 2009; Schieber and Chandel, 2013). In addition, UCB-MSCs treated with H_2O_2 have the ability to enhance epidermal reorganization, restoring the normal wound microarchitecture almost completely. Therefore, elucidating the role of H_2O_2 in the regulation of MMP12 and ECM proteins may offer important insights to improve our understanding of the role of the microenvironment in MSCs transplantation and regeneration of injured tissue. Thus, the regulation and/or maintenance of the optimum H_2O_2 concentration during clinical applications might be a novel and powerful tool to modulate the motility of human UCB-MSCs. In conclusion, H_2O_2 stimulates the ERK/p38MAPK/NF-κB and ERK/GSK-3β/β-catenin pathways, which are essential for MMP12-mediated COL-5 and FN degradation, and promotes human UCB-MSCs motility.

Acknowledgements

This research was supported by National R&D Program through the National Research Foundation of Korea (NRF) funded by the Ministry of Science, ICT & Future Planning (NRF-2013M3A9B4076520) and by a grant from the Next-Generation BioGreen 21 Program (No.PJ009090), Rural Development Administration, Republic of Korea.

Conflict of interest

The authors declare no conflict of interest.

References

Allaoui A, Botteaux A, Dumont JE, Hoste C, De Deken X (2009). Dual oxidases and hydrogen peroxide in a complex dialogue between host mucosae and bacteria. Trends Mol Med 15: 571–579.

Alexander SPH, Benson HE, Faccenda E, Pawson AJ, Sharman JL, Spedding M *et al*. (2013). The Concise Guide to PHARMACOLOGY 2013/14: Enzymes. Br J Pharmacol 170: 1797–1867.

Atkins RJ, Stylli SS, Luwor RB, Kaye AH, Hovens CM (2013). Glycogen synthase kinase-3beta (GSK-3β) and its dysregulation in glioblastoma multiforme. J Clin Neurosci 20: 1185–1192.

Bai XC, Deng F, Liu AL, Zou ZP, Wang Y, Ke ZY *et al*. (2002). Phospholipase C- γ1 is required for cell survival in oxidative stress by protein kinase C. Biochem J 363: 395–401.

Barnes MJ, Farndale RW (1999). Collagens and atherosclerosis. Exp Gerontol 34: 513–525.

Bourboulia D, Han H, Jensen-Taubman S, Gavil N, Isaac B, Wei B *et al*. (2013). TIMP-2 modulates cancer cell transcriptional profile and enhances E-cadherin/β-catenin complex expression in A549 lung cancer cells. Oncotarget 4: 163–173.

Brett CM, Washington CB, Ott RJ, Gutierrez MM, Giacomini KM (1993). Interaction of nucleoside analogues with the sodium-nucleoside transport system in brush border membrane vesicles from human kidney. Pharm Res 10: 423–426.

Burdon RH (1995). Superoxide and hydrogen peroxide in relation to mammalian cell proliferation. Free Radic Biol Med 18: 775–794.

Cai H (2005). Hydrogen peroxide regulation of endothelial function: origins, mechanisms, and consequences. Cardiovasc Res 68: 26–36.

Chieng-Yane P, Bocquet A, Letienne R, Bourbon T, Sablayrolles S, Perez M *et al*. (2011). Protease-activated receptor-1 antagonist F 16618 reduces arterial restenosis by down-regulation of tumor necrosis factor alpha and matrix metalloproteinase 7 expression, migration, and proliferation of vascular smooth muscle cells. J Pharmacol Exp Ther 336: 643–651.

Cox B, Emili A (2006). Tissue subcellular fractionation and protein extraction for use in mass-spectrometry-based proteomics. Nat Protoc 1: 1872–1878.

Craig R, Larkin A, Mingo AM, Thuerauf DJ, Andrews C, McDonough PM *et al*. (2000). p38 MAPK and NF-κB collaborate to induce interleukin-6 gene expression and release. Evidence for a cytoprotective autocrine signaling pathway in a cardiac myocyte model system. J Biol Chem 275: 23814–23824.

Cuzzocrea S, Riley DP, Caputi AP, Salvemini D (2001). Antioxidant therapy: a new pharmacological approach in shock, inflammation, and ischemia/reperfusion injury. Pharmacol Rev 53: 135–159.

Dunsmore SE, Roes J, Chua FJ, Segal AW, Mutsaers SE, Laurent GJ (2001). Evidence that neutrophil elastase-deficient mice are resistant to bleomycin-induced fibrosis. Chest 120: 35S–36S.

Eble JA, Figueiredo de Rezende F (2014). Redox-relevant aspects of the extracellular matrix and its cellular contacts via integrins. Antioxid Redox Signal 20: 1977–1993.

Goldkorn T, Balaban N, Shannon M, Chea V, Matsukuma K, Gilchrist D *et al*. (1998). H_2O_2 acts on cellular membranes to generate ceramide signaling and initiate apoptosis in tracheobronchial epithelial cells. J Cell Sci 111 (Pt 21): 3209–3220.

Harris LK, Smith SD, Keogh RJ, Jones RL, Baker PN, Knofler M *et al*. (2010). Trophoblast- and vascular smooth muscle cell-derived MMP-12 mediates elastolysis during uterine spiral artery remodeling. Am J Pathol 177: 2103–2115.

Hautamaki RD, Kobayashi DK, Senior RM, Shapiro SD (1997). Requirement for macrophage elastase for cigarette smoke-induced emphysema in mice. Science 277: 2002–2004.

Henzler T, Steudle E (2000). Transport and metabolic degradation of hydrogen peroxide in *Chara corallina*: model calculations and measurements with the pressure probe suggest transport of H_2O_2 across water channels. J Exp Bot 51: 2053–2066.

Iglesias-De La Cruz MC, Ruiz-Torres P, Alcami J, Diez-Marques L, Ortega-Velazquez R, Chen S *et al*. (2001). Hydrogen peroxide increases extracellular matrix mRNA through TGF-β in human mesangial cells. Kidney Int 59: 87–95.

Irani K, Xia Y, Zweier JL, Sollott SJ, Der CJ, Fearon ER *et al*. (1997). Mitogenic signaling mediated by oxidants in Ras-transformed fibroblasts. Science 275: 1649–1652.

Jeong JA, Hong SH, Gang EJ, Ahn C, Hwang SH, Yang IH *et al*. (2005). Differential gene expression profiling of human umbilical cord blood-derived mesenchymal stem cells by DNA microarray. Stem Cells 23: 584–593.

Kang H, Lee M, Choi KC, Shin DM, Ko J, Jang SW (2012). N-(4-hydroxyphenyl)retinamide inhibits breast cancer cell invasion through suppressing NF-κB activation and inhibiting matrix metalloproteinase-9 expression. J Cell Biochem 113: 2845–2855.

Kawano S, Shoji S, Ichinose S, Yamagata K, Tagami M, Hiraoka M (2002). Characterization of Ca^{2+} signaling pathways in human mesenchymal stem cells. Cell Calcium 32: 165–174.

Kilkenny C, Browne W, Cuthill IC, Emerson M, Altman DG (2010). Animal research: reporting *in vivo* experiments: the ARRIVE guidelines. Br J Pharmacol 160: 1577–1579.

Kim MJ, Nepal S, Lee ES, Jeong TC, Kim SH, Park PH (2013). Ethanol increases matrix metalloproteinase-12 expression via NADPH oxidase-dependent ROS production in macrophages. Toxicol Appl Pharmacol 273: 77–89.

Kim SY, Lee JG, Cho WS, Cho KH, Sakong J, Kim JR *et al.* (2010). Role of NADPH oxidase-2 in lipopolysaccharide-induced matrix metalloproteinase expression and cell migration. Immunol Cell Biol 88: 197–204.

Kishibe M, Bando Y, Tanaka T, Ishida-Yamamoto A, Iizuka H, Yoshida S (2012). Kallikrein-related peptidase 8-dependent skin wound healing is associated with upregulation of kallikrein-related peptidase 6 and PAR2. J Invest Dermatol 132: 1717–1724.

Kumar A, Wu H, Collier-Hyams LS, Hansen JM, Li T, Yamoah K *et al.* (2007). Commensal bacteria modulate cullin-dependent signaling via generation of reactive oxygen species. EMBO J 26: 4457–4466.

Kurien BT, Scofield RH (2006). Western blotting. Methods 38: 283–293.

Lambeth JD, Krause KH, Clark RA (2008). NOX enzymes as novel targets for drug development. Semin Immunopathol 30: 339–363.

Lavigne MC, Eppihimer MJ (2005). Cigarette smoke condensate induces MMP-12 gene expression in airway-like epithelia. Biochem Biophys Res Commun 330: 194–203.

Le Belle JE, Orozco NM, Paucar AA, Saxe JP, Mottahedeh J, Pyle AD *et al.* (2011). Proliferative neural stem cells have high endogenous ROS levels that regulate self-renewal and neurogenesis in a PI3K/Akt-dependant manner. Cell Stem Cell 8: 59–71.

Le Blanc K, Tammik L, Sundberg B, Haynesworth SE, Ringden O (2003). Mesenchymal stem cells inhibit and stimulate mixed lymphocyte cultures and mitogenic responses independently of the major histocompatibility complex. Scand J Immunol 57: 11–20.

Lee do Y, Choi BK, Lee DG, Kim YH, Kim CH, Lee SJ *et al.* (2013). 4-1BB signaling activates the T cell factor 1 effector/β-catenin pathway with delayed kinetics via ERK signaling and delayed PI3K/AKT activation to promote the proliferation of $CD8^+$ T Cells. PLoS ONE 8: e69677.

Lee KB, Choi J, Cho SB, Chung JY, Moon ES, Kim NS *et al.* (2011). Topical embryonic stem cells enhance wound healing in diabetic rats. J Orthop Res 29: 1554–1562.

Lee SH, Na SI, Heo JS, Kim MH, Kim YH, Lee MY *et al.* (2009). Arachidonic acid release by H_2O_2 mediated proliferation of mouse embryonic stem cells: involvement of Ca^{2+}/PKC and MAPKs-induced EGFR transactivation. J Cell Biochem 106: 787–797.

Lee SH, Lee YJ, Han HJ (2010a). Effect of arachidonic acid on hypoxia-induced IL-6 production in mouse ES cells: involvement of MAPKs, NF-κB, and HIF-1α. J Cell Physiol 222: 574–585.

Lee SH, Lee YJ, Song CH, Ahn YK, Han HJ (2010b). Role of FAK phosphorylation in hypoxia-induced hMSCS migration: involvement of VEGF as well as MAPKS and eNOS pathways. Am J Physiol Cell Physiol 298: C847–C856.

Li S, Deng Y, Feng J, Ye W (2009). Oxidative preconditioning promotes bone marrow mesenchymal stem cells migration and prevents apoptosis. Cell Biol Int 33: 411–418.

Lidke DS, Huang F, Post JN, Rieger B, Wilsbacher J, Thomas JL *et al.* (2010). ERK nuclear translocation is dimerization-independent but controlled by the rate of phosphorylation. J Biol Chem 285: 3092–3102.

Loo AE, Wong YT, Ho R, Wasser M, Du T, Ng WT *et al.* (2012). Effects of hydrogen peroxide on wound healing in mice in relation to oxidative damage. PLoS ONE 7: e49215.

Ma C, Bower KA, Chen G, Shi X, Ke ZJ, Luo J (2008). Interaction between ERK and GSK3β mediates basic fibroblast growth factor-induced apoptosis in SK-N-MC neuroblastoma cells. J Biol Chem 283: 9248–9256.

Magnusson MK, Mosher DF (1998). Fibronectin: structure, assembly, and cardiovascular implications. Arterioscler Thromb Vasc Biol 18: 1363–1370.

McGrath J, Drummond G, McLachlan E, Kilkenny C, Wainwright C (2010). Guidelines for reporting experiments involving animals: the ARRIVE guidelines. Br J Pharmacol 160: 1573–1576.

Morimoto H, Iwata K, Ogonuki N, Inoue K, Atsuo O, Kanatsu-Shinohara M *et al.* (2013). ROS are required for mouse spermatogonial stem cell self-renewal. Cell Stem Cell 12: 774–786.

Niethammer P, Grabher C, Look AT, Mitchison TJ (2009). A tissue-scale gradient of hydrogen peroxide mediates rapid wound detection in zebrafish. Nature 459: 996–999.

Nikitovic D, Corsini E, Kouretas D, Tsatsakis A, Tzanakakis G (2013). ROS-major mediators of extracellular matrix remodeling during tumor progression. Food Chem Toxicol 61: 178–186.

Pan Q, Qiu WY, Huo YN, Yao YF, Lou MF (2011). Low levels of hydrogen peroxide stimulate corneal epithelial cell adhesion, migration, and wound healing. Invest Ophthalmol Vis Sci 52: 1723–1734.

Park JH, Han HJ (2009). Caveolin-1 plays important role in EGF-induced migration and proliferation of mouse embryonic stem cells: involvement of PI3K/Akt and ERK. Am J Physiol Cell Physiol 297: C935–C944.

Park JH, Ryu JM, Yun SP, Kim MO, Han HJ (2012). Fibronectin stimulates migration through lipid raft dependent NHE-1 activation in mouse embryonic stem cells: involvement of RhoA, Ca^{2+}/CaM, and ERK. Biochim Biophys Acta 1820: 1618–1627.

Peng WJ, Yan JW, Wan YN, Wang BX, Tao JH, Yang GJ *et al.* (2012). Matrix metalloproteinases: a review of their structure and role in systemic sclerosis. J Clin Immunol 32: 1409–1414.

Priyanka HP, Bala P, Ankisettipalle S, ThyagaRajan S (2013). *Bacopa monnieri* and L-deprenyl differentially enhance the activities of antioxidant enzymes and the expression of tyrosine hydroxylase and nerve growth factor via ERK 1/2 and NF-kappaB pathways in the spleen of female wistar rats. Neurochem Res 38: 141–152.

Qiao C, Xu W, Zhu W, Hu J, Qian H, Yin Q *et al.* (2008). Human mesenchymal stem cells isolated from the umbilical cord. Cell Biol Int 32: 8–15.

Schieber MS, Chandel NS (2013). ROS links glucose metabolism to breast cancer stem cell and EMT phenotype. Cancer Cell 23: 265–267.

Sensebe L, Krampera M, Schrezenmeier H, Bourin P, Giordano R (2010). Mesenchymal stem cells for clinical application. Vox Sang 98: 93–107.

Shirvaikar N, Marquez-Curtis LA, Janowska-Wieczorek A (2012). Hematopoietic stem cell mobilization and homing after transplantation: the role of MMP-2, MMP-9, and MT1-MMP. Biochem Res Int 2012: 685267.

Suh HN, Han HJ (2011). Collagen I regulates the self-renewal of mouse embryonic stem cells through α2β1 integrin- and DDR1-dependent Bmi-1. J Cell Physiol 226: 3422–3432.

Sundaresan M, Yu ZX, Ferrans VJ, Irani K, Finkel T (1995). Requirement for generation of H_2O_2 for platelet-derived growth factor signal transduction. Science 270: 296–299.

Wakitani S, Nawata M, Tensho K, Okabe T, Machida H, Ohgushi H (2007). Repair of articular cartilage defects in the patello-femoral joint with autologous bone marrow mesenchymal cell transplantation: three case reports involving nine defects in five knees. J Tissue Eng Regen Med 1: 74–79.

Wu WS, Wu JR, Hu CT (2008). Signal cross talks for sustained MAPK activation and cell migration: the potential role of reactive oxygen species. Cancer Metastasis Rev 27: 303–314.

Xiao Q, Luo Z, Pepe AE, Margariti A, Zeng L, Xu Q (2009). Embryonic stem cell differentiation into smooth muscle cells is mediated by Nox4-produced H_2O_2. Am J Physiol Cell Physiol 296: C711–C723.

Yang SE, Ha CW, Jung M, Jin HJ, Lee M, Song H *et al.* (2004). Mesenchymal stem/progenitor cells developed in cultures from UC blood. Cytotherapy 6: 476–486.

Yang XS, Liu SA, Liu JW, Yan Q (2012). Fucosyltransferase IV enhances expression of MMP-12 stimulated by EGF via the ERK1/2, p38 and NF-κB pathways in A431 cells. Asian Pac J Cancer Prev 13: 1657–1662.

Yoo MS, Shin JS, Choi HE, Cho YW, Bang MH, Baek NI *et al.* (2012). Fucosterol isolated from *Undaria pinnatifida* inhibits lipopolysaccharide-induced production of nitric oxide and pro-inflammatory cytokines via the inactivation of nuclear factor-κB and p38 mitogen-activated protein kinase in RAW264.7 macrophages. Food Chem 135: 967–975.

Yun SP, Lee MY, Ryu JM, Song CH, Han HJ (2009). Role of HIF-1α and VEGF in human mesenchymal stem cell proliferation by 17β-estradiol: involvement of PKC, PI3K/Akt, and MAPKs. Am J Physiol Cell Physiol 296: C317–C326.

Yun SP, Ryu JM, Park JH, Kim MO, Lee JH, Han HJ (2012). Prostaglandin E_2 maintains mouse ESC undifferentiated state through regulation of connexin31, connexin43 and connexin45 expression: involvement of glycogen synthase kinase 3β/β-catenin. Biol Cell 104: 378–396.

Supporting information

Additional Supporting Information may be found in the online version of this article at the publisher's web-site:

http://dx.doi.org/10.1111/bph.12681

Figure S1 The efficiency of *MMP12* knockdown. Protein levels of MMP12 in lysates of UCB-MSCs transfected with *MMP12* specific siRNA (200 pmol·L^{-1}) are shown. The knockdown efficacy of *MMP12* was >70%. Data represent means ± SEM of three independent experiments. *P < 0.05 versus control.

Figure S2 Effect of H_2O_2 on human UCB-MSCs motility. A typical time lapse imaging experiment shows directed migration of human UCB-MSC with treatment of H_2O_2. Each example shown is representative of five independent experiments.

Figure S3 Effect of mitomycin C on H_2O_2-induced cell migration. Wound-healing level of UCB-MSCs treated with mitomycin C is shown. Cells were pretreated with mitomycin C and then exposed to H_2O_2 treatment for 24 h. Data represent means ± SEM of five independent experiments with triplicate dishes. *P < 0.05 versus control. n.s., not significant.

Figure S4 Effect of H_2O_2 on [^{3}H]-thymidine incorporation. UCB-MSCs were synchronized by serum deprivation for 36 h and treated with 1 μM H_2O_2 for 24 h. [^{3}H]-thymidine incorporation was determined. Data represents the mean ± SEM of four independent experiments for each condition.

Figure S5 Effect of H_2O_2 on PKCα phosphorylation. Co-immunoprecipitation of p-PKC by PKCα was determined (top left panel). The bottom left panel shows immunoprecipitated PKCα. PKC phosphorylation and PKCα expression in cell lysates are shown in the right panels. n = 3.

Figure S6 The effect of *non-targeting* (*nt*) siRNA for *MMP12* siRNA on the degradation of COL-5 and FN in H_2O_2-treated UCB-MSCs. Protein levels of COL-5 and FN in lysates and cell culture supernatants of UCB-MSCs transfected with *nt* control siRNA (200 pmol·L^{-1}) are shown. n = 3.

Table S1 Primers used for polymerase chain reaction.

Table S2 siRNA sequence for transfection.

Table S3 Effect of H_2O_2 on cell proliferation.

Video S1 Cell migration at basal level.mpg.

Video S2 Cell migration induced by H_2O_2.mpg.